



MALT1 targeting suppresses CARD14-induced psoriatic dermatitis in mice

Elien Van Nuffel^{1,2}, Jens Staal^{1,2} , Griet Baudalet^{1,2}, Mira Haegman^{1,2}, Yasmine Driège^{1,2}, Tino Hochepped^{1,2}, Inna S Afonina^{1,2,†} & Rudi Beyaert^{1,2,*†} 

Abstract

CARD14 gain-of-function mutations cause psoriasis in humans and mice. Together with BCL10 and the protease MALT1, mutant CARD14 forms a signaling node that mediates increased NF- κ B signaling and proinflammatory gene expression in keratinocytes. However, it remains unclear whether psoriasis in response to CARD14 hyperactivation is keratinocyte-intrinsic or requires CARD14 signaling in other cells. Moreover, the *in vivo* effect of MALT1 targeting on mutant CARD14-induced psoriasis has not yet been documented. Here, we show that inducible keratinocyte-specific expression of CARD14^{E138A} in mice rapidly induces epidermal thickening and inflammation as well as increased expression of several genes associated with psoriasis in humans. Keratinocyte-specific MALT1 deletion as well as oral treatment of mice with a specific MALT1 protease inhibitor strongly reduces psoriatic skin disease in CARD14^{E138A} mice. Together, these data illustrate a keratinocyte-intrinsic causal role of enhanced CARD14/MALT1 signaling in the pathogenesis of psoriasis and show the potential of MALT1 inhibition for the treatment of psoriasis.

Keywords cytokines; inflammation; MALT1; psoriasis; therapeutic

Subject Categories Immunology; Molecular Biology of Disease; Skin

DOI 10.15252/embr.201949237 | Received 6 September 2019 | Revised 27

March 2020 | Accepted 31 March 2020 | Published online 28 April 2020

EMBO Reports (2020) 21: e49237

Introduction

Psoriasis is a skin disease with both autoinflammatory and autoimmune components that is characterized by red, scaly, and sharply demarcated plaques which appear in a relapsing, remitting pattern. It is a common disease which affects 2–3% of the world population. Furthermore, psoriasis is often linked with comorbidities such as psoriatic arthritis and imposes a heavy psychological burden [1,2]. Current therapies for psoriasis mainly consist of immunosuppressive small molecules such as cyclosporine and methotrexate, or biologics that target key cytokines such as IL-17a, IL-23, and TNF.

Even though the treatment options have increased over the past few years, they are still not effective for all patients, can be associated with unwanted side effects, and have a high production cost, demonstrating the need for alternative treatments [3].

According to the current view on the pathogenesis of psoriasis, the disease is mainly maintained by a pathogenic interplay between keratinocytes and immune cells such as dendritic cells, T cells, and neutrophils. Activation of dendritic cells in the skin results in IL-12 and IL-23 production, leading to recruitment and activation of Th17 cells, which produce inflammatory mediators such as IL-17a and TNF. These stimulate keratinocyte hyperproliferation and secretion of cytokines and chemokines, leading to further recruitment of immune cells and thus resulting in a chronic inflammatory loop [2]. However, the factors that kindle these processes are still not entirely clear.

Genetic effects play a substantial part in the etiology of psoriasis. This is illustrated by the strong association of several single nucleotide polymorphisms and psoriasis susceptibility loci (*PSORS*) with psoriasis [4]. *Caspase recruitment domain-containing protein 14* (*CARD14*) is a gene that is located in the *PSORS2* locus and for which several gain-of-function mutations have been associated with psoriasis and pityriasis rubra pilaris in humans [5–8]. Transgenic expression of psoriasis-associated mutants of *CARD14* leads to excessive proinflammatory signaling in keratinocytes *in vitro* [9,10], and heterozygous mice harboring mutant CARD14^{ΔE138}, CARD14^{E138A}, or CARD14^{ΔQ136} were recently shown to spontaneously develop a psoriatic phenotype [11,12]. CARD14, also known as CARMA2, is closely related to CARD9, CARD10 (CARMA3), and CARD11 (CARMA1) [13], which upon activation, each form an oligomeric CBM signaling complex with B-cell lymphoma 10 (BCL10) and mucosa-associated lymphoid tissue lymphoma translocation protein 1 (MALT1). In this CBM complex, MALT1 acts as a scaffold for other proteins that mediate NF- κ B and JNK/p38 MAP kinase signaling [9,10]. CBM complex formation also activates MALT1 protease activity, resulting in the cleavage of a limited number of substrates whose cleavage is believed to further fine-tune inflammatory signaling (reviewed in refs. [14] and [15]). The biological relevance of MALT1 protease activity is highlighted by the autoimmune phenotype of mice expressing catalytically inactive

1 VIB Center for Inflammation Research, Ghent, Belgium

2 Department of Biomedical Molecular Biology, Ghent University, Ghent, Belgium

*Corresponding author. Tel: +32 9 331 37 70; E-mail: rudi.beyaert@irc.vib-ugent.be

†These authors contributed equally to this work as senior authors

MALT1 (reviewed in ref. [16]). On the other hand, inhibition of MALT1 suppresses T- and B-cell activation and prevents disease development in preclinical models of autoimmune disease and oncogenic MALT1-driven lymphoma, illustrating the therapeutic potential of MALT1 inhibition [17–22].

We have previously demonstrated that inhibition of MALT1 proteolytic activity reduces $CARD14^{E138A}$ -induced secretion of inflammatory cytokines in primary human keratinocytes [9]. To further investigate whether targeting MALT1 might be a valid strategy in the treatment of psoriasis, we have created transgenic mice that inducibly express a human psoriasis-associated hyperactive $CARD14^{E138A}$ mutant specifically in keratinocytes [7] and tested the effect of genetic or pharmacological inhibition of MALT1. We show here that inducible expression of $CARD14^{E138A}$ in keratinocytes is sufficient to cause psoriasis-like skin inflammation in mice, illustrating a keratinocyte-intrinsic effect of $CARD14^{E138A}$. Using this elegant novel mouse model, we demonstrate that genetic deletion of MALT1 as well as oral treatment with a small compound MALT1 inhibitor suppresses $CARD14^{E138A}$ -induced psoriasiform inflammation, highlighting the therapeutic potential of MALT1 targeting for the treatment of psoriasis.

Results and Discussion

Keratinocyte-specific deletion of MALT1 reduces $CARD14^{E138A}$ -induced psoriasiform inflammation

Several $CARD14$ gain-of-function mutations have been identified in psoriasis patients, and mice with heterozygous expression of some of these mutants ($CARD14^{AE138}$, $CARD14^{E138A}$, or $CARD14^{AQ136}$) were recently shown to spontaneously develop a psoriatic phenotype [11,12]. To further investigate the physiological role of MALT1 in $CARD14$ -induced psoriatic disease, we analyzed the effect of MALT1 deficiency on the development of disease symptoms induced by keratinocyte-specific expression of the human $CARD14^{E138A}$ transgene in mice. The $CARD14^{E138A}$ mutation was chosen because it was identified in a patient with pustular psoriasis and displays potent activation of NF- κ B [7,9]. It was previously reported that mice carrying a similar mutation in the endogenous $Card14$ gene show increased mortality [11,12]. Although the reasons for this are still unclear, it is not unlikely that mutant $CARD14$ expression in different cell types or tissues besides skin keratinocytes, such as endothelial cells, $\gamma\delta$ T cells, Langerhans cells, esophagus, and colon, contributes to the observed lethality [5,23,24]. We therefore decided to generate conditional $CARD14^{E138A}$ transgenic mice by knocking in the human $CARD14^{E138A}$ cDNA preceded by a loxP-flanked stop cassette under control of the ROSA26 promoter using RMCE-mediated recombination [25] (Fig 1A), which were subsequently crossed with male mice expressing Cre recombinase under the keratin 5 (K5) promoter in order to obtain epidermal $CARD14^{E138A}$ expression in the skin [26]. Further crossing of these mice into mice containing a floxed (fl) $Malt1$ allele was done to obtain MALT1 deficiency in epidermal cells. We did not observe a normal mendelian segregation pattern in MALT1 sufficient conditions because no mice expressing both the K5cre transgene and $CARD14^{E138A}$ transgene were obtained (Fig 1B) ($P < 0.0001$, chi-square test). However, upon caesarian section, pups at E18.5 that

express the $CARD14^{E138A}$ transgene in skin tissue could be recovered (Fig 1C). Even though these pups did not show any overt phenotype and were indistinguishable compared to wild-type littermates (Fig 1D), they failed to survive longer than 24 h after birth. Toluidine blue staining showed that the epidermal skin barrier of $CARD14^{E138A}$ transgenic mice is intact and histological sections of the skin did not show clear abnormalities (Fig EV1A and B). Importantly, mice expressing epidermal $CARD14^{E138A}$ in the absence of MALT1 were born at expected mendelian segregation of the genotypes ($P = 0.9824$, chi-square test; Fig 1E) and did not show macroscopically visible signs of disease. Body weight and ear thickness of these mice were comparable to littermate controls, and histological analysis of ear and skin sections did not indicate epidermal thickening or inflammation in mice between 4 and 7 months old (Fig 1F–H). Immunohistochemistry staining for GFP confirmed expression of the bicistronic $CARD14^{E138A}/GFP$ transgene in the epidermis of the ears (Fig EV1C). Together, these data show that constitutive K5cre-driven $CARD14^{E138A}$ expression results in perinatal lethality and highlight an important *in vivo* role for MALT1 in $CARD14$ signaling. The quick onset of death of K5cre- $CARD14^{E138A}$ expressing pups is quite surprising and is unlikely to be attributed to $CARD14^{E138A}$ expression in the skin only (see also below).

Because the lethality induced by constitutive epidermal expression of $CARD14^{E138A}$ prevented us from analyzing the effect of MALT1 targeting on mutant $CARD14$ -induced psoriasis, we crossed $CARD14^{E138A}$ transgenic mice with mice containing a K14creER transgene, allowing the tamoxifen-inducible expression of $CARD14^{E138A}$ in stratified epithelia as found in skin and certain other tissues such as tongue and esophagus [27,28]. To account for possibly unanticipated effects of Cre expression, mice that contain the K14creER transgene but not the $CARD14^{E138A}$ transgene were used as wild-type controls (Fig 2A). Mice with both transgenes (hereafter referred to as inducible epidermal $CARD14^{E138A}$ (ie $CARD14^{E138A}$)) were born at normal mendelian ratios and did not show any sign of disease up to 6 weeks of age. From 6 weeks on, some mild but significant swelling of the ears was observed in ie $CARD14^{E138A}$ mice in the absence of tamoxifen, which might be caused by leaky expression of the $CARD14^{E138A}$ transgene due to marginal spontaneous K14creER activity. Otherwise, the mice were healthy and did not show differences in body weight (Fig EV2A). To investigate the effect of MALT1 deficiency, we also generated ie $CARD14^{E138A}$ mice with floxed $Malt1$ alleles, which allow $CARD14^{E138A}$ induction together with MALT1 deletion in epidermal cells upon tamoxifen treatment (hereafter referred to as $Malt1^{EKO}$ ie $CARD14^{E138A}$ mice). Similar to $Malt1^{+/+}$ ie $CARD14^{E138A}$ mice, $Malt1^{EKO}$ ie $CARD14^{E138A}$ mice showed mild ear thickening before treatment with tamoxifen (Fig EV2B). It should be mentioned that complete Cre-mediated MALT1 deletion requires two recombination events, while only a single recombination is needed for $CARD14^{E138A}$ transgene expression. Therefore, the minor leaky K14creER activity may not be sufficient to induce complete MALT1 deletion in the absence of tamoxifen. In addition, due to MALT1 protein stability, MALT1 protein expression levels do not diminish as fast as $CARD14^{E138A}$ protein expression levels rise. Tamoxifen treatment of $Malt1^{+/+}$ ie $CARD14^{E138A}$ mice increased ear swelling progressively (twofold), and the ears became red and scaly (Figs 2B and EV2C). Furthermore, ie $CARD14^{E138A}$ mice showed a rapid decrease in body weight, up to 18 percent, 4 days after tamoxifen

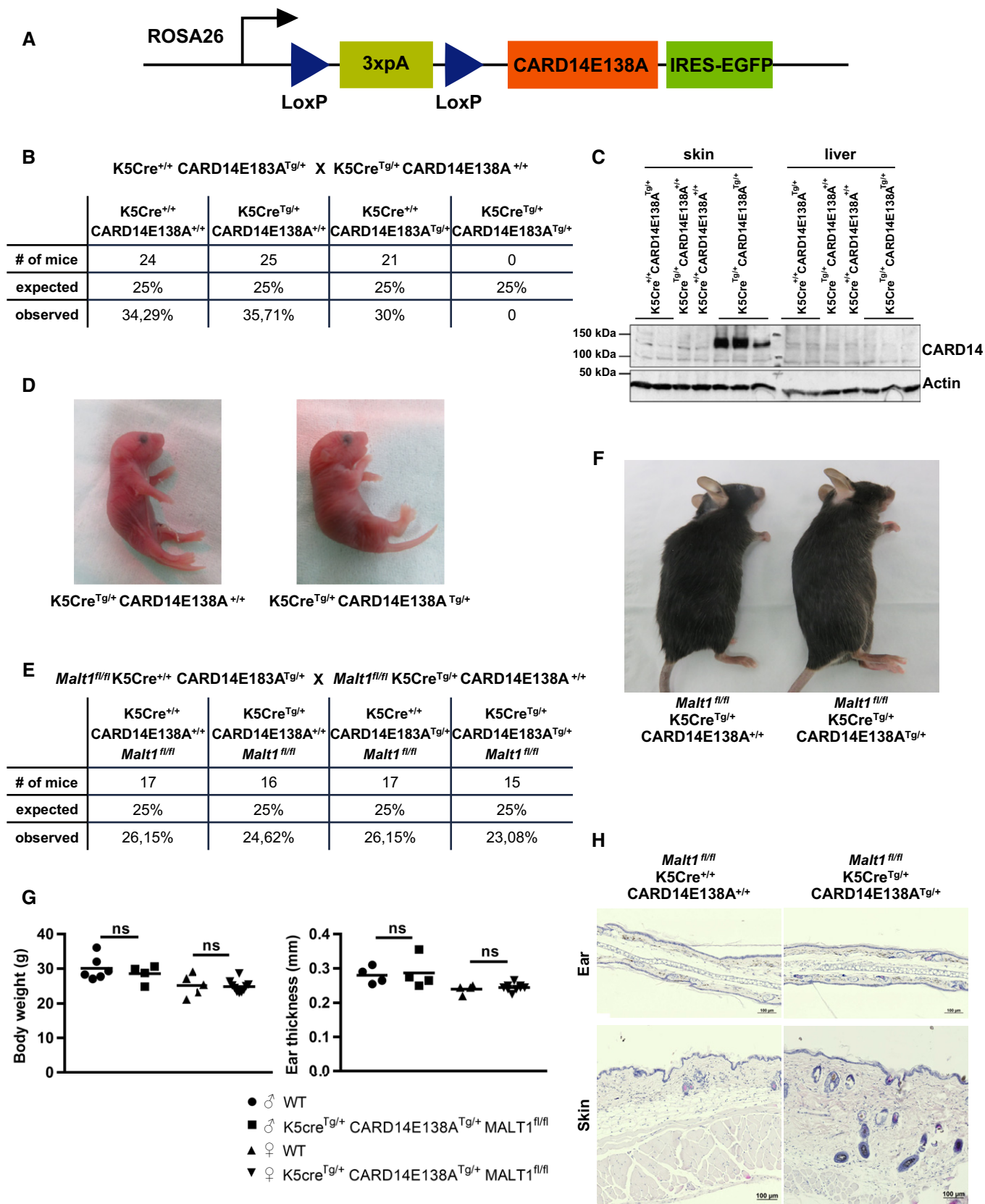


Figure 1.

Figure 1. Perinatal lethality of CARD14E138A transgenic mice is rescued by MALT1 deficiency.

- A Schematic representation of the Rosa26^{LSL-CARD14-E138A} transgene construct (LSL = LoxP-stop-LoxP).
- B Ratio of genotypes obtained of 1-week-old pups after crossing K5cre^{Tg/+} CARD14E138A^{+/+} male mice with K5cre^{+/+} CARD14E138A^{Tg/+} female mice; CARD14E138A^{+/+} = Rosa26^{+/+}, CARD14E138A^{Tg/+} = Rosa26^{LSL-CARD14-E138A/+}.
- C Representative Western blot showing CARD14 protein levels in skin and liver lysates of E18.5 pups. Actin is shown as a loading control.
- D Representative images of K5cre^{Tg/+} CARD14E138A^{+/+} and K5cre^{Tg/+} CARD14E138A^{Tg/+} pups at E18.5.
- E Ratio of genotypes obtained of 1-week-old pups from crossing *Malt1*^{fl/fl} K5cre^{Tg/+} CARD14E138A^{+/+} male mice with *Malt1*^{fl/fl} K5cre^{+/+} CARD14E138A^{Tg/+} female mice.
- F Representative image of 6-month-old *Malt1*^{fl/fl} K5cre^{Tg/+} CARD14E138A^{+/+} and *Malt1*^{fl/fl} K5cre^{Tg/+} CARD14E138A^{Tg/+} mice.
- G Body weight and ear thickness of untreated WT and *Malt1*^{fl/fl} K5cre^{Tg/+} CARD14E138A^{Tg/+} male and female mice (between 4 and 7 months old). Each symbol represents one mouse; the line represents the mean value ($n \geq 4$ mice per group). WT = *Malt1*^{fl/fl} K5cre^{+/+} CARD14E138A^{+/+}, *Malt1*^{fl/fl} K5cre^{+/+} CARD14E138A^{Tg/+}, and *Malt1*^{fl/fl} K5cre^{Tg/+} CARD14E138A^{+/+} mice. Statistical difference between two groups was determined using a Mann–Whitney U-test (ns: $P > 0.05$).
- H Representative H&E-stained histological sections of ear and skin tissue of *Malt1*^{fl/fl} K5cre^{+/+} CARD14E138A^{+/+} and *Malt1*^{fl/fl} K5cre^{Tg/+} CARD14E138A^{Tg/+} mice (scale bar represents 100 μm).

Source data are available online for this figure.

administration, at which point mice were euthanized to minimize suffering (Fig 2B). It should be mentioned that no clear macroscopic signs of psoriatic disease could be observed at other skin regions 4 days after tamoxifen treatment.

In contrast to the clear psoriatic phenotype of *Malt1*^{+/+} ieCARD14^{E138A} mice in the ears, increased ear swelling and loss of body weight were much less pronounced in tamoxifen-treated *Malt1*^{EKO} ieCARD14^{E138A} mice (Fig 2B), indicating an important role for MALT1. Hematoxylin and eosin staining of ear sections showed acanthosis, hyperkeratosis, and parakeratosis in *Malt1*^{+/+} ieCARD14^{E138A} mice, which are histological features of human psoriasis (Fig 2C) [2,29]. In line with this, blinded measurements showed that the thickness of the epidermis was significantly increased and also immunostaining for Ki67, a marker for proliferation, showed an increased amount of proliferating cells in the basal layer of ear skin of *Malt1*^{+/+} ieCARD14^{E138A} mice (Figs 2D and EV2D). Furthermore, several large infiltrates of immune cells, reminiscent of Munro's abscesses, were visible in the stratum corneum (Fig 2C, arrowheads). Thickening of the epidermis and inflammatory cell infiltration in the stratum corneum were reduced in *Malt1*^{EKO} ieCARD14^{E138A} mice compared to *Malt1*^{+/+} ieCARD14^{E138A} mice (Fig 2C and D). Flow cytometry analysis of the ears showed that neutrophils are one of the most abundant infiltrating immune cell types, which is consistent with the large pustules observed in ear sections and the acute nature of our model (Fig 2E). Also T cells and dendritic cells were increased, while the amount of eosinophils,

which are associated with Th2 immunity, remained very low. Again, the number of infiltrating neutrophils and dendritic cells was significantly reduced in the ears of *Malt1*^{EKO} ieCARD14^{E138A} mice (Fig 2E).

mRNA analysis of the ears of *Malt1*^{+/+} ieCARD14^{E138A} mice showed a strong induction of proinflammatory cytokines and chemokines that are strongly linked to and expressed during human psoriasis, such as *Il17a*, *Il23*, *Il36 γ* , *Cxcl1*, *Cxcl2*, and *Tnf* (Fig 2F) [30]. Furthermore, expression of antimicrobial peptides such as *S100a8* and *Lcn2*, which are also highly increased in human psoriatic lesions, was upregulated (Fig 2F) [31]. As expected, human transgene *CARD14*^{E138A} mRNA levels were high in ieCARD14^{E138A} mice and absent in wild-type mice (Fig 2F). Most importantly, upregulation of most of the analyzed cytokines, chemokines, and antimicrobial peptides was much less pronounced in ears of MALT1-deficient ieCARD14^{E138A} mice (Fig 2F). Of note, *Il17a* mRNA levels were similar in *Malt1*^{EKO} ieCARD14^{E138A} and *Malt1*^{+/+} ieCARD14^{E138A} mice, which might reflect equal T-cell counts in the ears of both mouse lines (Fig 2E and F). Both the chemokines CXCL1 and CXCL2 and the antimicrobial peptide LCN2 have been shown to recruit and modulate neutrophil activation and in this way contribute to psoriatic inflammation [32,33]. Therefore, the reduced *Cxcl1/2* and *Lcn2* levels are in line with the reduced neutrophil influx in ears of *Malt1*^{EKO} ieCARD14^{E138A} mice and might explain the protective effect of MALT1 deficiency. Taken together, our data demonstrate that human *CARD14*^{E138A} expression in keratinocytes is sufficient to drive a pathogenic inflammatory cascade

Figure 2. Keratinocyte-specific deletion of MALT1 reduces CARD14E138A-induced psoriasiform inflammation.

- A Schematic representation of the experimental induction of CARD14^{E138A} transgene using tamoxifen. WT = K14creER^{Tg/+} Rosa26^{+/+}, ieCARD14^{E138A} = K14creER^{Tg/+} Rosa26^{LSL-CARD14-E138A/+}.
- B Changes in relative body weight and ear thickness upon CARD14^{E138A} induction with tamoxifen. *Malt1*^{EKO} = *Malt1*^{fl/fl}. The combined results of five independent experiments are shown (*Malt1*^{+/+} WT $n = 17$, *Malt1*^{fl/fl} WT $n = 8$, *Malt1*^{+/+} ieCARD14^{E138A} $n = 18$, *Malt1*^{fl/fl} ieCARD14^{E138A} $n = 12$).
- C Representative H&E-stained histological sections of ear tissue of tamoxifen-treated mice (scale bar represents 200 μm). Arrowheads indicate infiltrates of immune cells.
- D Epidermal thickness measured on ear sections. Each symbol represents the mean of at least ten measurements for each ear; the line represents the mean value. The combined results of three independent experiments are shown.
- E Analysis of infiltrating immune cells in the ears of tamoxifen-treated mice using flow cytometry. Cell count of neutrophils (CD45⁺ CD3/CD19⁻ CD64⁻ CD11b⁺ Ly6G⁺), eosinophils (CD45⁺ CD3/CD19⁻ CD64⁻ Ly6G⁻ SiglecF⁺), T cells (CD45⁺ CD3/CD19⁺, MHCII⁻), and DCs (CD45⁺ CD3/CD19⁻ CD64⁻ MHCII⁺CD11c⁺) in single cell suspensions of the ear ($n \geq 4$).
- F mRNA expression levels of the indicated genes in ears relative to reference genes (*Hprt1*, *Rpl13a*, and *Tbp1*). Each symbol represents one mouse; the line represents the mean value ($n \geq 3$).

Data information: Statistics: Error bars reflect SEM. Differences between *Malt1*^{+/+} ieCARD14^{E138A} and *Malt1*^{EKO} ieCARD14^{E138A} groups were determined using REML analysis (B) or a Mann–Whitney U-test (D–F) (* $P < 0.05$, ** $P < 0.01$, **** $P < 0.0001$).

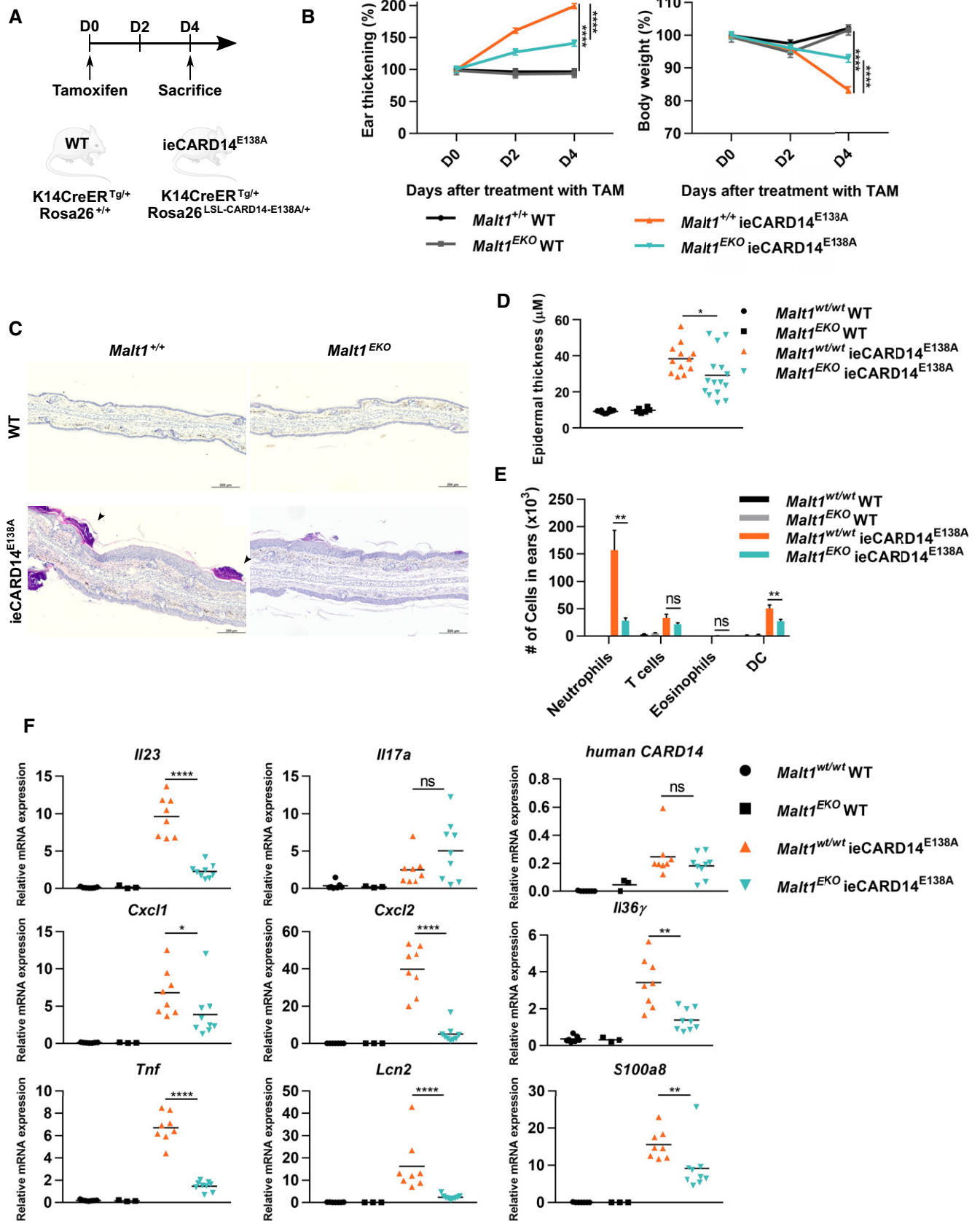


Figure 2.

mimicking several pathological features of human psoriasis. Most importantly, our data are the first to demonstrate a keratinocyte-intrinsic *in vivo* role of MALT1 in skin inflammation. However, it should be mentioned that the above described protective effect of MALT1 deletion on CARD14^{E138A}-induced skin inflammation does not allow us to distinguish between the role of MALT1 scaffold versus MALT1 proteolytic activities.

The quick onset of death of CARD14^{E138A} expressing pups as well as the rapid weight loss of up to 18% over 4 days of tamoxifen-induced transgene induction in ieCARD14^{E138A} mice can hardly be attributed to health problems in the skin only. Closer examination showed that the stomach of ieCARD14^{E138A} mice was less filled and that blood glucose levels were lower 4 days after tamoxifen treatment (Fig EV3A and B), suggesting a defect in eating behavior. We could not detect a significant difference in body temperature (Fig EV3C) or transepidermal water loss through the skin (Fig EV3D). It should be mentioned that K14creER has been shown to not only target keratinocytes of the skin, but also keratinocytes of the oral epithelia, tongue, and esophagus, as well as mammary epithelium, vaginal epithelium, salivary glands, and cornea [27,28]. As high-quality antibodies against CARD14 that can be used for immunohistochemistry are not available, we performed immunohistochemistry for GFP, which is expressed with CARD14^{E138A} as a bicistronic transgene (Fig 1A). This revealed that the transgene is not only expressed in the ears, but also in the stratified epithelium of the tongue and the epithelium of salivary glands, and very faintly in the esophagus (Fig EV3E). In addition, we could detect clear infiltration of CD45⁺ inflammatory cells in the tongue (Fig EV3E). Together these results let us speculate that epithelial expression of the CARD14^{E138A} transgene in the oral epithelium induces inflammatory reactions that lead to irritation and affect eating behavior and weight loss of ieCARD14^{E138A} mice. Similar effects may also explain the observed mortality in pups in which CARD14^{E138A} expression is under control of K5cre.

Inhibition of MALT1 proteolytic activity attenuates CARD14^{E138A}-induced psoriasis

Therapeutic targeting of MALT1 proteolytic activity by small compound inhibitors has shown promising effects in preclinical models of inflammatory disease and cancer [17–22]. However,

therapeutic targeting of MALT1 in the context of psoriasis has not yet been reported. The inducible and rapidly developing skin phenotype of ieCARD14^{E138A} mice as well as the causal link with a mutation present in humans makes these mice particularly interesting to test the effect of MALT1 small compound inhibitors in psoriatic dermatitis. We therefore investigated the effect of systemic treatment with MLT-827, a potent small compound inhibitor of MALT1 proteolytic activity that has been originally developed by Novartis [34], on the development of psoriasiform dermatitis in ieCARD14^{E138A} mice. MALT1 is ubiquitously expressed, and systemic treatment with a small compound MALT1 inhibitor is expected to affect MALT1 activity in different cell types that may contribute to disease development, including keratinocytes and T cells. MLT-827 was administered two times daily by oral gavage, starting at the same time as tamoxifen treatment (Fig 3A). It should be mentioned that due to some leaky CARD14^{E138A} expression, mice already exhibit increased ear thickness before tamoxifen and MALT1 inhibitor treatment. Using immunoblot analysis of ear tissue extracts, we could show that CARD14^{E138A} expression induces cleavage of CYLD and BCL10, two known substrates of MALT1 [35,36]. Cleavage of both substrates was completely prevented in mice treated with the MALT1 inhibitor MLT-827 (Fig 3B), illustrating *in vivo* MALT1 target engagement of the compound. Compared to vehicle-treated mice, MALT1 inhibitor treatment almost completely blocked ear swelling induced by CARD14^{E138A} and reduced the accompanying loss in body weight (Fig 3C). In line with this, hematoxylin and eosin staining of ear sections showed that the epidermis is less thickened in MALT1 inhibitor-treated mice (Fig 3D and E). However, the reduction in epidermal thickening was rather limited compared to the strong reduction in total ear thickness, suggesting that reduced ear swelling mainly reflects reduced edema and inflammatory cell infiltration in the skin. Next, we examined inflammatory cytokine secretion by lymphocytes of the ear-draining lymph nodes of mice treated with MLT-827. CD3/CD28-induced IL-6 and IL-17a production was significantly lower in the lymphocytes isolated from MALT1 inhibitor-treated mice when compared to vehicle-treated mice (Fig 3F), suggesting that MALT1 inhibition can impair the development of a Th17-response in CARD14^{E138A}-induced psoriasis. Consistent with our earlier results, mRNA levels encoding several proinflammatory mediators were strongly upregulated in ears of vehicle-treated ieCARD14^{E138A} mice (Figs 3G and EV4), which was significantly diminished in MLT-827

Figure 3. Inhibition of MALT1 proteolytic activity attenuates CARD14^{E138A}-induced psoriasis.

- A Schematic representation of the experimental set-up of CARD14^{E138A} induction and MALT1 inhibitor treatment.
- B Cleavage of MALT1 substrates CYLD and BCL10 as analyzed by Western blotting of lysates of ear tissue of mice 4 days after treatment with tamoxifen and MALT1 inhibitor or vehicle. Actin is shown as a loading control. Each lane represents one mouse.
- C Changes in relative ear thickness and body weight in vehicle- and MALT1 inhibitor-treated mice upon CARD14^{E138A} induction. M1 inh = MALT1 inhibitor, WT = K14creER^{Tg/+} Rosa26^{+/+}, ieCARD14^{E138A} = K14creER^{Tg/+} Rosa26^{LSL-CARD14-E138A/+}. Combined results of two independent experiments are shown (WT + vehicle: $n = 9$, WT + M1 inh: $n = 8$, ieCARD14^{E138A} + vehicle: $n = 9$, ieCARD14^{E138A} + M1 inh: $n = 10$).
- D, E (D) Representative histological sections of ear tissue stained with hematoxylin and eosin and (E) measurements of epidermal thickness of tamoxifen-treated mice. Combined results of two independent experiments are shown. Each symbol represents the mean of at least ten epidermal thickness measurements for each ear; the line represents the mean value.
- F IL-6 and IL-17a production by ear-draining lymphocytes upon *ex vivo* restimulation with anti-CD3/anti-CD28 for 3 days ($n \geq 3$ biological replicates).
- G Heatmap showing relative mRNA expression levels of the indicated genes in ear tissue normalized to reference genes. Values represent median of each group ($n \geq 3$).

Data information: Statistics: Data are representative for two independent experiments. Error bars reflect SEM. *P*-values were determined using REML analysis (C), two-way ANOVA with Sidak correction for multiple comparisons (D), or a Mann–Whitney *U*-test (E) (**P* < 0.05, ****P* < 0.001, *****P* < 0.0001). Source data are available online for this figure.

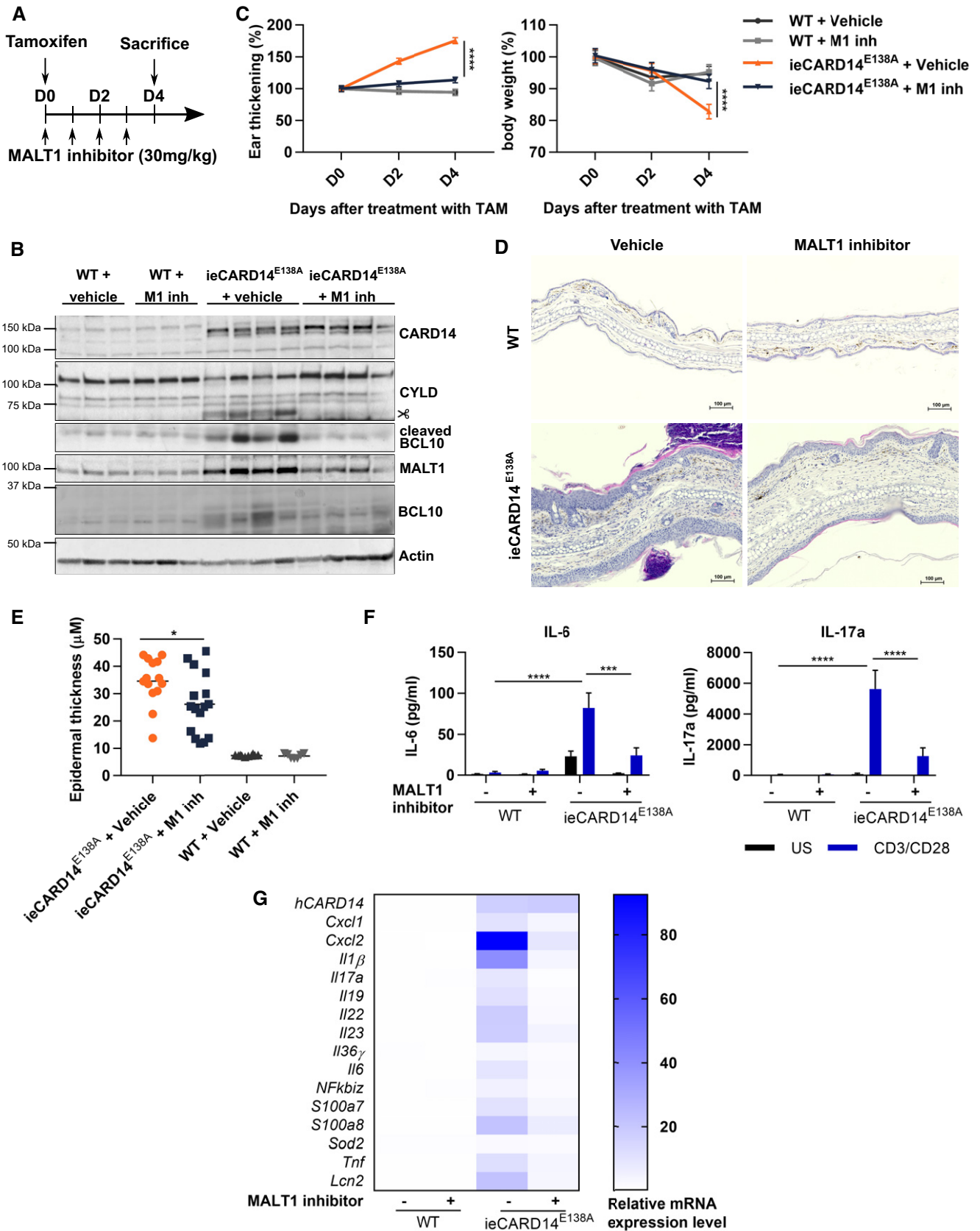


Figure 3.

treated mice. In particular, the strong inhibition of *Il17a*, *Il23*, *Cxcl1*, and *Tnf* expression by MLT-827 demonstrates that MALT1 inhibition can tackle psoriasis-like inflammation induced by CARD14^{E138A}. Furthermore, also the expression of other cytokines such as *Il36γ*, *Il1β*, and *Il6* and antimicrobial peptides such as *S100a8* and *Lcn2* was significantly reduced upon MALT1 inhibitor treatment in CARD14^{E138A} mice (Figs 3F and EV4). Together, these data show that MALT1 proteolytic activity plays a key role in CARD14^{E138A}-induced psoriasiform dermatitis and illustrate that MALT1 inhibitor treatment may be an interesting novel therapeutic approach in psoriasis. It should be mentioned that in our mouse model MLT-827 treatment is not only targeting MALT1 in keratinocytes, but also other cell types that play a role in skin inflammation. For example, T-cell receptor-induced MALT1 activation mediates T-cell proliferation and Th17 differentiation [19,22,37], while MALT1 proteolytic activity has also been shown to regulate endothelial permeability and activation [38,39]. Therefore, MALT1 inhibition might attenuate CARD14^{E138A}-induced skin inflammation at multiple levels. Interestingly, a few early reports describe amelioration of psoriasis features in psychiatric patients treated with the antipsychotic chlorpromazine, which was recently shown to also inhibit MALT1 [40–42], further supporting the use of MALT1 inhibitors for the management of psoriasis. Furthermore, accumulating evidence suggests a more ubiquitous role for CARD14-MALT1 signaling axis in inflammatory skin conditions. For instance, CARD14 mutations have not only been identified in psoriasis patients but also in patients suffering from pityriasis rubra pilaris, a rare inflammatory skin disease phenotypically related to psoriasis [5], indicating that MALT1 targeting may also be of interest in psoriasis-related skin diseases. Noteworthy, while dominant gain-of-function mutations in CARD14 are associated with psoriasis and related diseases, loss-of-function mutations in CARD14 were recently reported to be associated with a severe variant of atopic dermatitis [43]. It will be interesting to investigate the effect of MALT1 targeting in the context of atopic dermatitis to obtain a complete view on the potential of MALT1 targeting in inflammatory skin disease. Of note, several groups have shown that mice expressing a catalytically inactive MALT1 mutant suffer from multiorgan inflammation and autoimmunity, likely caused by a reduced frequency of regulatory T cells [19,37,44–46]. In contrast, pharmacological inhibition of MALT1 in preclinical mouse models did not lead to obvious side effects, suggesting that MALT1 inhibitor treatment may be safe [18,20]. Genetic inactivation of MALT1 may indeed not be representative for pharmacological inhibition of MALT1 as the latter may affect less the development of regulatory T cells in the thymus and never lead to a complete MALT1 inhibition. Nevertheless, it will be important to closely monitor possible side effects upon long-term systemic treatment with MALT1 inhibitors. Alternatively, in the case of psoriasis, it might also be possible to deliver MALT1 inhibitors topically, with less risk of systemic side effects.

Materials and Methods

Rosa26^{LSL-CARD14-E138A} transgenesis

Cloning of RMCE targeting constructs

Plasmids of the cloned genes were deposited in the BCCM/GeneCorner plasmid collection along with detailed descriptions of

cloning strategy and plasmid sequence (<http://bccm.belspo.be/ab-out-us/bccm-genecorner>). Human CARD14^{E138A} (LMBP : 9623) was cloned into pENTR3C. The ENTR clone was integrated in the pDV1_RMCE (LMBP: 8870) destination vector using Gateway LR reactions to generate a RMCE targeting vector for CARD14E138A (LMBP: 09578).

RMCE targeting

RMCE compatible mouse ES cells (G4 ROSALUC [25]) were cultured in standard ES-cell medium containing 500 ml Knock-out™-DMEM (Thermo Fisher Scientific) supplemented with 15% FBS (Hyclone), 100 μM non-essential amino acids (Thermo Fisher Scientific), 1× GlutaMAX (Thermo Fisher Scientific), 100 μM β-mercaptoethanol (Thermo Fisher Scientific), and 2,000 U/ml leukemia inhibitory factor (Protein Service Facility, VIB). ES cells were co-transfected with 2.5 μg of a FipE expressing plasmid and 2.5 μg of targeting vector using lipofectamin 2000 (Thermo Fisher Scientific) according to the manufacturer's instructions [47]. G418 selection (200 μg/ml) was applied 48 h after transfection. After 7–10 days, individual G418-resistant, RMCE-targeted ES-cell clones were picked and further expanded. Correct targeting events were confirmed by PCR; the targeted allele generates a band of 560 bp (primers: FW 5' AAA GTC GCT CTG AGT TGT TAT 3' and REV 5' GCG GCC TCG ACT CTA CGA TA 3'), as previously described [25]. Correctly targeted ES cells were aggregated with outbred Swiss morula, which were then implanted into pseudopregnant Swiss mice to generate chimeric mice that transmitted the transgene to their offspring.

Mice

Mice were bred and maintained under specific pathogen-free conditions and housed in individually ventilated cages in accordance with the institutional and national guidelines regarding the care and use of laboratory animals. Animal protocols were approved by the ethics committee of Ghent University (EC2017_013, EC2017_102, and EC2018_056). To induce Cre excision of the Lox-STOP-Lox (LSL) cassette, hemizygous Rosa26^{LSL-CARD14-E138A} transgenic mice were bred with hemizygous K5cre and K14creER mouse strains. This generated double transgenic mice that constitutively express CARD14^{E138A} transgene or express CARD14^{E138A} transgene inducibly upon tamoxifen treatment in epidermal cells [26,27]. As controls, littermates that only express the K5cre or K14creER transgene were used.

Malt1^{tm1a(EUCOMM)Hmg/+} (C57BL6/N background) mice were derived from ES cells purchased from EUCOMM. *Malt1* *tm1a* mice were bred with mice of the FLP deleter strain (C57BL6/J background) to remove the FRT-flanked LacZ and neomycin selection cassette and to generate the *Malt1* *tm1c* floxed allele [48]. *Malt1* *tm1c* mice were bred with Rosa26^{LSL-CARD14-E138A} transgenic and K5Cre or K14creER transgenic mouse strains to obtain mice with CARD14^{E138A}-transgene-expressing, MALT1-deficient keratinocytes. To induce expression of the CARD14^{E138A} transgene, both male and female mice of 8–9 weeks old were injected intraperitoneally with 2.5 mg tamoxifen (T-5648, Sigma-Aldrich) dissolved in corn oil (C8267, Sigma-Aldrich). Mice were weighed, and ear thickness was measured every other day using a G-1A dial thickness gauge (Peacock, Japan) by an observer blinded to the treatments and

genotypes. For MALT1 inhibitor treatment, mice were treated two times per day using oral gavage with 30 mg/kg MALT1 inhibitor (MLT-827; generously provided by Galapagos n.v., Mechelen) dissolved in Kolliphor[®] HS 15 (42966, Sigma)/methylcellulose 0.5% (AX021233, VWR chemicals) (2/98% ratio) under continuous stirring and protected from light.

Genotyping

The *Malt1* floxed allele or knockout allele was genotyped with the primers MALTcKO-F (GTTTCTCAGGCTTTAGTTCATGTC), CoMLT-3-R (TATACTCTACATCTCCATGGT), and MALTcKO-R (TTGTTT TGCAGATCTCTGCC) resulting in 280 bp (WT), 448 bp (FL), and 345 (KO) products. Rosa26^{LSL-CARD14E138A} transgenes were genotyped using the following primers: Fwd 5' AACCTGACGTCTACACCCT 3', Rev 5' CACTCGGTCAGCTTGGATGT 3' resulting in a 95 bp PCR product.

Histology

Ears, skin, tongue, salivary gland, and esophagus were dissected and incubated in 4% PFA in PBS at 4°C overnight, followed by dehydration and embedding in paraffin. Sections of 5 µm were deparaffinized followed by staining with hematoxylin and eosin. For immunohistochemistry staining, antigen retrieval was performed by heating the slides in a citrate-based antigen unmasking solution (H-3300, Vector Laboratories) and endogenous peroxidase activity was blocked by immersing slides in 3% H₂O₂. Nonspecific binding was blocked by incubating sections in 5% normal goat serum and 1% BSA. The following primary antibodies were used: anti-GFP (2956, Cell Signaling Technology), anti-CD45 (ab10558, Abcam), and anti-Ki67 (12202, Cell Signaling Technology). After overnight incubation with the primary antibody at 4°C, the tissue sections were sequentially incubated with a biotinylated anti-rabbit secondary Ab (E0432, Dako), followed by incubation with Vectastain Elite ABC kit (PK-6100, Vector Laboratories), followed by detection with diaminobenzidine chromogen (ImmPACT[®] DAB, SK-4105, Vector Laboratories) and counterstaining with hematoxylin. Sections were mounted by use of Entellan mounting medium (Merck Millipore). Images were acquired with Axio Scan.Z1 slide scanner (Zeiss), and image analysis was done using Zen lite (Zeiss) software. Average epidermal thickness was determined as the mean of at least 10 measurements for each sample.

Cytokine production by lymphocytes

For CD3/CD28 stimulation, a 96-well plate was coated overnight at 4°C with 200 µl PBS containing 1 µg/ml anti-CD3 (553057, BD Biosciences) and 1 µg/ml anti-CD28 (553294, BD Biosciences). Single cell suspensions from ear-draining lymph nodes were obtained by homogenizing the lymph node through a 70 µm cell sieve. Isolated lymphocytes were counted, and 200,000 lymphocytes were seeded in an anti-CD3/CD28-coated plate for *in vitro* restimulation. After 72 h, the medium was collected and assayed for IL-6 (171-G5007M) and IL-17a (171-G5013M) production by Bio-Plex Pro (Bio-Rad) according to manufacturer's instructions on a Bio-Plex 200 system (Bio-Rad).

Western blotting

After sacrifice, ears or back skin were harvested and immediately frozen and stored at -70°C. To make protein lysates, tissues were homogenized and lysed using Precellys 24 (Bertin technologies with CK26 beads) in Laemmli buffer (50 mM Tris-HCl pH 8, 2% SDS, 10% glycerol). Debris was removed by two centrifugation steps at 16,000 g for 10 min. Pierce[™] BCA Protein Assay Kit (23225, Thermo Fisher Scientific) was used to determine protein concentration. 0.005% bromophenol blue and 5% β-mercaptoethanol were added to the samples, and equal amounts of proteins were loaded and separated by 10% SDS-PAGE. Proteins were then transferred to nitrocellulose membrane with 0.45 µm pores (Protran, Perkin Elmer). The membranes were blocked in 5% milk powder in TBS/0.2% Tween 20 (TBST) for 1 h at room temperature (RT) and probed with specific primary antibodies in 5% milk powder in TBST. The following antibodies were used: anti-CARD14 (10400-1-AP, Proteintech), anti-CYLD (sc-74435, Santa Cruz), anti-BCL10 cleavage-specific (gift from Thijs Baens, Cistim Leuven vzw, Leuven, Belgium), anti-BCL10 (sc-5273, Santa Cruz), anti-MALT1 (32494, Cell Signaling Technology), and anti-β-actin-HRP (sc-47778, Santa Cruz). Secondary HRP-conjugated anti-mouse or anti-rabbit IgG antibody was purchased from Thermo Fisher Scientific (31432 and 31464). Proteins were detected using the Western Lightning ECL detection system (Perkin Elmer) according to the manufacturer's instructions.

RNA extraction, cDNA synthesis, and quantitative real-time PCR

After sacrifice, ears were harvested at the base and incubated overnight in RNA later at 4°C before long-term storage at -70°C. For RNA extraction, ears were homogenized and lysed using Precellys 24 (Bertin technologies with CK26 beads) in TRIzol reagent (Invitrogen). After phenol-chloroform phase separation, RNA was isolated using RNeasy mini kit (Qiagen). Synthesis of cDNA was performed using an iScript Advanced cDNA synthesis kit (Bio-Rad), according to manufacturer's instructions. Quantitative PCR was performed with a LightCycler 480 (Roche) using SensiFAST[™] SYBR[®] No-ROX kit (Bioline) with a total of 10 ng of cDNA and 300 nM of specific primers in a total volume of 10 µl. Real-time PCR reactions were performed in triplicates. The following specific primers were used (5'-3'): *Hprt1* forward, AGTGTGGATACAGGCCAGAC; *Hprt1* reverse, CGTGATTCAAATCCCTGAAGT; *Tbp* forward, TCTACCG TGAATCTTGGCTGTAAA; *Tbp* reverse, TTCTCATGATGACTGCAGC AAA; *Rpl13a* forward, CCTGCTGCTCTCAAGTT; *Rpl13a* reverse, TGGTTGCTACTGCCTGGTACTT; *Il17a* forward, GGACTCTCCACCGC AATGA; *Il17a* reverse, TCAGGCTCCCTCTTCAGGAC; *Il23* forward, CCCGTATCCAGTGTGAAGATG; *Il23* reverse, GGGCTATCAGGG AGTAGAGCA; *Il1f9 (Il36γ)* forward, TCCTGACTTTGGGGAGGTT TT; *Il1f9 (Il36γ)* reverse, TCACGCTGACTGGGGTACT; *hCARD14* forward, GTCAACACGGACGGTTATAAGA; *hCARD14* reverse, GT TGACCCGGATGTAGAATGAG; *S100a7a* forward, TGCTCTTGATA GTGTGCCTC; *S100a7a* reverse, GCTCTGTGATGTAGTATGGCTG; *Ccl20* forward, GTACTGCTGGCTCACCTCTG; *Ccl20* reverse, CTTCA TCGGCCACTCTCTTGTG; *Cxcl1* forward, GAGCCTCTAACAGTT CCAG; *Cxcl1* reverse, TGAGTGTGGCTATGACTTCG; *Cxcl2* forward, ACAGAAGTCATAGCCACTCTC; *Cxcl2* reverse, TTAGCCTTGCC TTTGTTTCAG; *Tnf* forward, ACCCTGGTATGAGCCATATAC; *Tnf*

reverse, ACACCCATTCCCTTCACAGAG; *Il1 β* forward, CACCTCA CAAGCAGAGCACAAAG; *Il1 β* reverse, GCATTAGAAACAGTCCAGC CCATAC; *Il19* forward, CTCCTGGGCATGACGTTGATT; *Il19* reverse, GCATGGCTCTCTTGATCTCGT; *Il22* forward, CAGCTCCTGTCACA TCAGCGGT; *Il22* reverse, AGGTCCAGTTCCCAATCGCCT; *Il6* forward, GAGGATACCACTCCCAACAGACC; *Il6* reverse, AAGTGCA TCATCGTTGTTTCATACA; *S100a8* forward, AAATCACCATGCCTCT ACAAG; *S100a8* reverse, CCCACTTTTATCACCATCGCAA; *S100a9* forward, ATACTCTAGGAAGGAAGGACACC; *S100a9* reverse, TCCA TGATGTCATTTATGAGGGC; *Lcn2* forward, TGGCCCTGAGTGTC A TGTG; *Lcn2* reverse CTCTGTAGCTCATAGATGGTGC; and *Sod2* forward, CAGACCTGCCTTACGACTATGG; *Sod2* reverse CTCGGTG GCGTTGAGATTGTT. Analysis was done using qBase+ software (Biogazelle, Gent, Belgium). Values were normalized to the appropriate amount of reference genes, as determined by geNorm analysis in the qBase software.

Flow cytometry

Ear samples were incubated overnight at 4°C with 200 μ g/ml Dispase II (from Bacillus polymerase grade 2; Roche) with the dermal side down to facilitate isolation of cells. Next, the ear skin was manually minced into small pieces and was further digested with 1.5 mg/ml collagenase type 4 (Worthington Biochemical, Lakewood, NJ) and 10 U of DNase (Roche) in RPMI medium buffered with HEPES and supplemented with 2% FCS. The suspension was resuspended for 30 min and provided with fresh digestion buffer for a total of 90 min at 37°C. After digestion, the cell suspension was passed through 100 and 40 μ m cell strainers to remove debris and clots.

For phenotyping of immune cells in cell suspensions of ear skin, cells were stained with CD16/CD32 (553142, BD), MHCII-eFluor 450 (# 48-5321-80, eBioscience), CD64-BV711 (Biolegend, 139311), Siglec F-PE (BD, 552126), CD45-APC-eFluor780 (47-0451-82, eBioscience), CD8-PerCP-Cy5.5 (45-0081, eBioscience), CD3-PE-Cy5 (55-0031, Tonbo Biosciences), CD19-PE-Cy5 (15-0193, eBioscience), CD11c-PE-Cy7 (117317, Biolegend), CD11b-BV605 (563015, BD), $\gamma\delta$ -TCR-APC (17-5711, eBioscience), Ly6G-AF700 (561236, BD), and CD4-APC-eFluor780 (47-0042, eBioscience). Dead cells were excluded from the analysis by using fixable viability dye eFluor506 (eBioscience), and 123count eBeads (01-1234-42, Invitrogen) were used for quantification of cells. Acquisition of multi-color samples was done on an LSRFortessa flow cytometer (BD Bioscience). Final analysis and graphical output were performed using FlowJo software (Tree Star Inc.).

Statistical analysis

Results are expressed as mean \pm SEM. Statistical analysis between two groups was done with GraphPad Prism 7 using a Mann–Whitney *U*-test for unpaired data. Analysis of data from Bio-Plex analysis was performed with GraphPad Prism 7 using two-way ANOVA to determine significant differences. Relative body weight and ear thickness measured at consecutive equally spaced time points were analyzed as repeated measurements data (also called longitudinal data) using the residual maximum likelihood (REML) as implemented in Genstat v19 [49]. Briefly, a linear mixed model (random terms underlined) of the form $y = \mu + \text{genotype} + \text{time} +$

$\text{genotype.time} + \text{replicate} + \text{mouse.time}$ was fitted to the longitudinal data. The term *mouse.time* represents the residual error term with dependent errors because the repeated measurements are taken in the same individual, causing correlations among observations. Times of measurement were set as equally spaced, and the autoregressive model of order 1 was selected as the best correlation model based on the Aikake information coefficient. Significances of genotype effects across time (i.e., *genotype.time*) and of pairwise differences between genotype effects across time were assessed by an approximate *F*-test, of which the denominator degrees of freedom were calculated using algebraic derivatives as implemented in Genstat v19.

Data availability

Plasmids were deposited in the BCCM/GeneCorner plasmid collection along with detailed descriptions of cloning strategy and plasmid sequence (<http://bccm.belspo.be/about-us/bccm-gene-corner>). All other data are available from the authors upon reasonable requests.

Expanded View for this article is available online.

Acknowledgments

We thank Galapagos n.v. for providing MLT-827. M. Baens is acknowledged for providing cleaved BCL10 specific antibody. This work was supported by grants from the VIB, the Research Foundation—Flanders (FWO) (G035517N and G090914N), the Foundation Against Cancer (FAF-F/2016/812), and the Ghent University Concerted Research Actions (GOA). I.S.A. is supported by a postdoctoral fellowship and research grants (1503418N and 1503815N) of the FWO. E.V.N. is supported by a predoctoral fellowship of the FWO. Marnik Vuylsteke is acknowledged for help and advice with the statistical analysis. We also thank prof. Wim Declercq for kindly providing K5cre and K14creER transgenic mice. Julie Deckers is acknowledged for advice on flow cytometry analysis and we are grateful to Kelly Lemeire for performing Ki67 immunohistochemistry staining on tissue sections.

Author contributions

EVN, JS, ISA, and RB contributed to the conception and design of the study. EVN, JS, TH, and ISA acquired the data. MH, GB, and YD provided technical assistance. EVN, JS, ISA, and RB analyzed and interpreted the data. EVN, JS, ISA, and RB drafted the article or revised it critically for important intellectual content. All authors approved the final version of the manuscript.

Conflict of interest

R.B. is inventor on a patent application (Inhibitors of MALT1 proteolytic activity and uses thereof; WO09065897; applicants: VIB and UGent) and was involved in a research collaboration with Galapagos n.v. that is no longer running. The authors have no additional financial interests.

References

- Connor CJ, Liu V, Fiedorowicz JG (2015) Exploring the physiological link between psoriasis and mood disorders. *Dermatol Res Pract* 2015: 409637
- Lowes MA, Suarez-Farinas M, Krueger JG (2014) Immunology of psoriasis. *Annu Rev Immunol* 32: 227–255

3. Hawkes JE, Chan TC, Krueger JG (2017) Psoriasis pathogenesis and the development of novel targeted immune therapies. *J Allergy Clin Immunol* 140: 645–653
4. Capon F (2017) The genetic basis of psoriasis. *Int J Mol Sci* 18: 2526
5. Fuchs-Telem D, Sarig O, van Steensel MA, Isakov O, Israeli S, Nousbeck J, Richard K, Winnepenninckx V, Vernooij M, Shomron N et al (2012) Familial pityriasis rubra pilaris is caused by mutations in CARD14. *Am J Hum Genet* 91: 163–170
6. Jordan CT, Cao L, Roberson ED, Duan S, Helms CA, Nair RP, Duffin KC, Stuart PE, Goldgar D, Hayashi G et al (2012) Rare and common variants in CARD14, encoding an epidermal regulator of NF- κ B, in psoriasis. *Am J Hum Genet* 90: 796–808
7. Jordan CT, Cao L, Roberson ED, Pierson KC, Yang CF, Joyce CE, Ryan C, Duan S, Helms CA, Liu Y et al (2012) PSORS2 is due to mutations in CARD14. *Am J Hum Genet* 90: 784–795
8. Van Nuffel E, Schmitt A, Afonina IS, Schulze-Osthoff K, Beyaert R, Hailfinger S (2017) CARD14-mediated activation of paracaspase MALT1 in keratinocytes: implications for psoriasis. *J Invest Dermatol* 137: 569–575
9. Afonina IS, Van Nuffel E, Baudelet G, Driege Y, Kreike M, Staal J, Beyaert R (2016) The paracaspase MALT1 mediates CARD14-induced signaling in keratinocytes. *EMBO Rep* 17: 914–927
10. Howes A, O'Sullivan PA, Breyer F, Ghose A, Cao L, Krappmann D, Bowcock AM, Ley SC (2016) Psoriasis mutations disrupt CARD14 autoinhibition promoting BCL10-MALT1-dependent NF- κ B activation. *Biochem J* 473: 1759–1768
11. Mellett M, Meier B, Mohanan D, Schairer R, Cheng P, Satoh TK, Kiefer B, Ospelt C, Nobbe S, Thome M et al (2018) CARD14 gain-of-function mutation alone is sufficient to drive IL-23/IL-17-mediated psoriasiform skin inflammation *in vivo*. *J Invest Dermatol* 138: 2010–2023
12. Wang M, Zhang S, Zheng G, Huang J, Songyang Z, Zhao X, Lin X (2018) Gain-of-function mutation of Card14 leads to spontaneous psoriasis-like skin inflammation through enhanced keratinocyte response to IL-17A. *Immunity* 49: 66–79.e65
13. Staal J, Driege Y, Haegman M, Borghi A, Hulpiau P, Lievens L, Gul IS, Sundararaman S, Goncalves A, Dhondt I et al (2018) Ancient origin of the CARD-Coiled Coil/Bcl10/MALT1-like paracaspase signaling complex indicates unknown critical functions. *Front Immunol* 9: 1136
14. Juilland M, Thome M (2018) Holding all the CARDS: how MALT1 controls CARMA/CARD-dependent signaling. *Front Immunol* 9: 1927
15. Ruland J, Hartjes L (2019) CARD-BCL-10-MALT1 signalling in protective and pathological immunity. *Nat Rev Immunol* 19: 118–134
16. Demeyer A, Staal J, Beyaert R (2016) Targeting MALT1 proteolytic activity in immunity, inflammation and disease: good or bad? *Trends Mol Med* 22: 135–150
17. Fontan L, Qiao Q, Hatcher JM, Casalena G, Us I, Teater M, Durant M, Du G, Xia M, Bilchuk N et al (2018) Specific covalent inhibition of MALT1 paracaspase suppresses B cell lymphoma growth. *J Clin Invest* 128: 4397–4412
18. Fontan L, Yang C, Kabaleeswaran V, Volpon L, Osborne MJ, Beltran E, Garcia M, Cerchietti L, Shaknovich R, Yang SN et al (2012) MALT1 small molecule inhibitors specifically suppress ABC-DLBCL *in vitro* and *in vivo*. *Cancer Cell* 22: 812–824
19. Jaworski M, Marsland BJ, Gehrig J, Held W, Favre S, Luther SA, Perroud M, Golshayan D, Gaide O, Thome M (2014) Malt1 protease inactivation efficiently dampens immune responses but causes spontaneous autoimmunity. *EMBO J* 33: 2765–2781
20. Mc Guire C, Elton L, Wieghofer P, Staal J, Voet S, Demeyer A, Nagel D, Krappmann D, Prinz M, Beyaert R et al (2014) Pharmacological inhibition of MALT1 protease activity protects mice in a mouse model of multiple sclerosis. *J Neuroinflammation* 11: 124
21. Nagel D, Spranger S, Vincendeau M, Grau M, Raffegerst S, Kloos B, Hlahla D, Neuenschwander M, Peter von Kries J, Hadian K et al (2012) Pharmacologic inhibition of MALT1 protease by phenothiazines as a therapeutic approach for the treatment of aggressive ABC-DLBCL. *Cancer Cell* 22: 825–837
22. Nakamura Y, Igaki K, Komoike Y, Yokoyama K, Tsuchimori N (2019) Malt1 inactivation attenuates experimental colitis through the regulation of Th17 and Th1/17 cells. *Inflamm Res* 68: 223–230
23. Harden JL, Lewis SM, Pierson KC, Suarez-Farinas M, Lentini T, Ortenzio FS, Zaba LC, Goldbach-Mansky R, Bowcock AM, Lowes MA (2014) CARD14 expression in dermal endothelial cells in psoriasis. *PLoS One* 9: e111255
24. Tanaka M, Kobiyama K, Honda T, Uchio-Yamada K, Natsume-Kitatani Y, Mizuguchi K, Kabashima K, Ishii KJ (2018) Essential role of CARD14 in murine experimental psoriasis. *J Immunol* 200: 71–81
25. Haenebalcke L, Goossens S, Naessens M, Kruse N, Farhang Chahremani M, Bartunkova S, Haigh K, Pieters T, Dierickx P, Drogat B et al (2013) Efficient ROSA26-based conditional and/or inducible transgenesis using RMCE-compatible F1 hybrid mouse embryonic stem cells. *Stem Cell Rev* 9: 774–785
26. Ramirez A, Page A, Gandarillas A, Zanet J, Pibre S, Vidal M, Tusell L, Genesca A, Whitaker DA, Melton DW et al (2004) A keratin K5Cre transgenic line appropriate for tissue-specific or generalized Cre-mediated recombination. *Genesis* 39: 52–57
27. Vasioukhin V, Degenstein L, Wise B, Fuchs E (1999) The magical touch: genome targeting in epidermal stem cells induced by tamoxifen application to mouse skin. *Proc Natl Acad Sci USA* 96: 8551–8556
28. Wang X, Zinkel S, Polonsky K, Fuchs E (1997) Transgenic studies with a keratin promoter-driven growth hormone transgene: prospects for gene therapy. *Proc Natl Acad Sci USA* 94: 219–226
29. Tirumalae R (2013) Psoriasiform dermatoses: microscopic approach. *Indian J Dermatol* 58: 290–293
30. Chiricozzi A, Romanelli P, Volpe E, Borsellino G, Romanelli M (2018) Scanning the immunopathogenesis of psoriasis. *Int J Mol Sci* 19: E179
31. Morizane S, Gallo RL (2012) Antimicrobial peptides in the pathogenesis of psoriasis. *J Dermatol* 39: 225–230
32. De Filippo K, Dudeck A, Hasenberg M, Nye E, van Rooijen N, Hartmann K, Gunzer M, Roers A, Hogg N (2013) Mast cell and macrophage chemokines CXCL1/CXCL2 control the early stage of neutrophil recruitment during tissue inflammation. *Blood* 121: 4930–4937
33. Shao S, Cao T, Jin L, Li B, Fang H, Zhang J, Zhang Y, Hu J, Wang G (2016) Increased Lipocalin-2 contributes to the pathogenesis of psoriasis by modulating neutrophil chemotaxis and cytokine secretion. *J Invest Dermatol* 136: 1418–1428
34. Bardet M, Unterreiner A, Malinverni C, Lafossas F, Vedrine C, Boesch D, Kolb Y, Kaiser D, Gluck A, Schneider MA et al (2018) The T-cell fingerprint of MALT1 paracaspase revealed by selective inhibition. *Immunol Cell Biol* 96: 81–99
35. Rebeaud F, Hailfinger S, Posevitz-Fejfar A, Tapernoux M, Moser R, Rueda D, Gaide O, Guzzardi M, Iancu EM, Rufer N et al (2008) The proteolytic activity of the paracaspase MALT1 is key in T cell activation. *Nat Immunol* 9: 272–281
36. Staal J, Driege Y, Bekaert T, Demeyer A, Muyliaert D, Van Damme P, Gevaert K, Beyaert R (2011) T-cell receptor-induced JNK activation requires proteolytic inactivation of CYLD by MALT1. *EMBO J* 30: 1742–1752

37. Yu JW, Hoffman S, Beal AM, Dykon A, Ringenberg MA, Hughes AC, Dare L, Anderson AD, Finger J, Kasparcova V et al (2015) MALT1 protease activity is required for innate and adaptive immune responses. *PLoS One* 10: e0127083
38. Klei LR, Hu D, Panek R, Alfano DN, Bridwell RE, Bailey KM, Oravec-Wilson KI, Concel VJ, Hess EM, Van Beek M et al (2016) MALT1 protease activation triggers acute disruption of endothelial barrier integrity via CYLD cleavage. *Cell Rep* 17: 221–232
39. Li Y, Huang S, Huang X, Li X, Falcon A, Soutar A, Bornancin F, Jiang Z, Xin HB, Fu M (2018) Pharmacological inhibition of MALT1 protease activity suppresses endothelial activation via enhancing MCP1P1 expression. *Cell Signal* 50: 1–8
40. D'Silva JL, Fisher RA (1956) Chlorpromazine in the management of psoriasis. *Ill Med J* 110: 135–136
41. Jacobs KA, Andre-Gregoire G, Maghe C, Thys A, Li Y, Harford-Wright E, Trillet K, Douanne T, Alves Nicolau C, Frenel JS et al (2020) Paracaspase MALT1 regulates glioma cell survival by controlling endo-lysosome homeostasis. *EMBO J* 39: e102030
42. Shimamoto Y, Shimamoto H (1990) Annular pustular psoriasis associated with affective psychosis. *Cutis* 45: 439–442
43. Peled A, Sarig O, Sun G, Samuelov L, Ma CA, Zhang Y, Dimaggio T, Nelson CG, Stone KD, Freeman AF et al (2019) Loss-of-function mutations in caspase recruitment domain-containing protein 14 (CARD14) are associated with a severe variant of atopic dermatitis. *J Allergy Clin Immunol* 143: 173–181.e110
44. Bornancin F, Renner F, Touil R, Sic H, Kolb Y, Touil-Allaoui I, Rush JS, Smith PA, Bigaud M, Junker-Walker U et al (2015) Deficiency of MALT1 paracaspase activity results in unbalanced regulatory and effector T and B cell responses leading to multiorgan inflammation. *J Immunol* 194: 3723–3734
45. Gewies A, Gorka O, Bergmann H, Pechloff K, Petermann F, Jeltsch KM, Rudelius M, Kriegsmann M, Weichert W, Horsch M et al (2014) Uncoupling Malt1 threshold function from paracaspase activity results in destructive autoimmune inflammation. *Cell Rep* 9: 1292–1305
46. Demeyer A, Skordos I, Driège Y, Kreike M, Hochepped T, Baens M, Staal J, Beyaert R (2019) MALT1 proteolytic activity suppresses autoimmunity in a T cell intrinsic manner. *Front Immunol* 10: 1898
47. Schaft J, Ashery-Padan R, van der Hoeven F, Gruss P, Stewart AF (2001) Efficient FLP recombination in mouse ES cells and oocytes. *Genesis* 31: 6–10
48. Rodriguez CI, Buchholz F, Galloway J, Sequerra R, Kasper J, Ayala R, Stewart AF, Dymecki SM (2000) High-efficiency deleter mice show that FLP is an alternative to Cre-loxP. *Nat Genet* 25: 139–140
49. VSN International (2017) *Genstat for Windows*, 19th edn. Hemel Hempstead, UK: VSN International. Genstat.co.uk